Fragmentation dynamics of argon clusters (Ar[sub n], n=2 to 11) following electron-impact ionization: Modeling and comparison with experiment

David Bonhommeau, Nadine Halberstadt, Alexandra Viel

Fragmentation dynamics of argon clusters (Ar_n, $n=2$ to 11) following electron-impact ionization: Modeling and comparison with experiment

David Bonhommeau and Nadine Halberstadt[a)]
Laboratoire de Physique Quantique, IRSAMC, UMR 5626, CNRS et Université P. Sabatier, F-31062, Toulouse cedex 09, France

Alexandra Viel
PALMS-SIMPA, UMR 6627 du CNRS, Université de Rennes 1, Campus de Beaulieu, F-35042 Rennes, France

(Received 24 February 2006; accepted 17 March 2006; published online 11 May 2006)

The fragmentation dynamics of argon clusters ionized by electron impact is investigated for initial cluster sizes up to $n=11$ atoms. The dynamics of the argon atoms is modeled using a mixed quantum-classical method in which the nuclei are treated classically and the transitions between electronic states quantum mechanically. The potential-energy surfaces are derived from a diatomics-in-molecules model with the addition of the induced dipole-induced dipole and spin-orbit interactions. The results show extensive and fast fragmentation. The dimer is the most abundant ionic fragment, with a proportion increasing from 66% for $n=2$ to a maximum of 95% for $n=6$ and then decreasing down to 67% for $n=11$. The next abundant fragment is the monomer for $n<7$ and the trimer otherwise. The parent ion dissociation lifetimes are all in the range of 1 ps. Long-lived trajectories appear for initial cluster sizes of seven and higher, and favor the formation of the larger fragments (trimers and tetramers). Our results show quantitative agreement with available experimental results concerning the extensive character of the fragmentation: Ar^+ and Ar_2^+ are the only ionic fragments for sizes up to five atoms; their overall proportion is in quantitative agreement for all the studied sizes; Ar_2^+ is the main fragment for all sizes; stable Ar_3^+ fragments only appear for $n \geqslant 5$, and their proportion increases smoothly with cluster size from there. However, the individual ionic monomer and dimer fragment proportions differ. The experimental ones exhibit oscillations with initial cluster size, with a slight tendency to decrease on average for the monomer. In contrast our results show a monotonic, systematic evolution, similar to what was found in our earlier studies on neon and krypton clusters. Several hypotheses are discussed in order to find the origin of this discrepancy. Finally, the metastable $II(1/2)_u$ and $II(1/2)_g$ states of Ar_2^+ are found to decay with a lifetime of 3.5 and 0.1 ps, respectively, due to spin-orbit coupling. The difference with the commonly accepted microsecond range value for rare-gas dimer ions could originate from the role of autoionizing states in the formation of the parent ions. © *2006 American Institute of Physics*. [DOI: 10.1063/1.2194552]

I. INTRODUCTION

Rare-gas clusters are simple systems, intermediate between molecules and solids. Despite their simplicity, they exhibit a wealth of interesting properties. In particular, it was recognized early on that their ionization induces extensive fragmentation.[1–5] This is due to the large difference in bonding nature between the neutral cluster, of Van der Waals type with small interaction energy and large bond lengths, and the ionic cluster with much larger interaction energy and smaller bond lengths. Hence upon vertical ionization the parent ions are created in a configuration very far from equilibrium, which gives them a lot of potential energy and induces fragmentation.

The main difficulty from the experimental point of view is that the supersonic expansions in which clusters are generated always produce a distribution of sizes. This makes it difficult to deduce the fragmentation pattern from a neutral cluster of a given size. Early experiments relied on the variation of expansion parameters such as backing pressure or nozzle orifice to change the maximum of the size distribution.[6] A crucial experiment to achieve neutral cluster size selection was performed by Buck and Meyer.[1,3] They exploited the different kinematic behavior of the neutral clusters in a scattering experiment in which the rare-gas cluster beam was crossed by a beam of helium atoms. The different species were separated by measuring their angular and velocity distributions. Their results revealed extensive fragmentation, with the trimer totally fragmenting to dimers and monomers, and all clusters with size $n=4-6$ appearing at the dimer ion mass with a relative probability to the trimer of 0.95 or more (the monomer channel could not be measured for these sizes). Their results were completed to include monomer fragments and extended up to $n=9$ by Lohbrandt *et al.*[7] This study confirmed the first measurements, and highlighted the extensive character of the fragmentation. The

[a)]Electronic mail: nadine.halberstadt@irsamc.ups-tlse.fr

TABLE I. Parameters in a.u. of the analytic curves for the four lowest molecular states of Ar_2^+ [Eqs. (1)–(4)]: all parameters result from fitting the *ab initio* points of Ha *et al.* (Ref. 23).

State	$^2\Sigma_u^+$	$^2\Pi_g$	$^2\Pi_u$	$^2\Sigma_g^+$
A_1	-2.2084×10^2	-6.6963×10^2	-5.5259×10^2	1.1547×10^1
α_1	2.2061	2.3898	2.6664	1.0839
B_1	0 (fixed)	-1.5376×10^{-4}	-8.8695×10^{-5}	-1.0130×10^{-2}
β_1	⋯	-1.3183×10^1	-1.8883×10^1	−4.2742
A_2	0 (fixed)	0 (fixed)	0 (fixed)	2.5810
α_2	⋯	⋯	⋯	2.5206×10^{-1}
B_2	0 (fixed)	0 (fixed)	0 (fixed)	1.2331×10^{-2}
β_2	⋯	⋯	⋯	-2.0168×10^1
D_1	−5.6694	−2.5561	-3.5230×10^{-1}	0 (fixed)
D_2	1.8403×10^2	3.6394×10^2	1.9030×10^2	0 (fixed)
δ	8.7310×10^{-1}	9.5169×10^{-1}	8.7349×10^{-1}	⋯
a	1.7197	1.9661	1.2935	6.6693×10^{-1}
b	8.2976	7.8110	8.3279	1.2183×10^1
C_4 (fixed)[a]	−5.32	−5.32	−5.32	−5.32
C_6	2.9606×10^2	1.0461×10^1	-3.1234×10^1	-2.6196×10^2
C_8	-9.4418×10^4	-1.2518×10^4	2.1703×10^3	4.3138×10^4

[a]Obtained by fitting the average of the asymptotic parts of the 4 curves to C_4/R^4, and held fixed at this value during the fit of the other coefficients.

dominant channel for all measured sizes up to $n=9$, except for $n=4$, was the dimer ion Ar_2^+, and no tetramer ions were observed within experimental uncertainties for this size range. A very recent experiment has been conducted on krypton clusters[8] using the same experimental conditions, and also shows extensive fragmentation.

From the theoretical point of view, only a few studies have been conducted on the fragmentation of rare-gas clusters upon ionization. Soler *et al.*[9] have conducted model calculations on argon, krypton, and xenon cluster ionization by assuming the initial formation of a dimer ion and simulating the subsequent evolution of the system using classical dynamics. This study was completed by Saenz *et al.*[10] who showed an appreciable boiling off of argon atoms. Their results were confirmed by Stampfli,[11] who studied the fragmentation of neon and xenon clusters upon ionization using classical dynamics on the ground electronic state. His results showed that there was always fragmentation for the trimers. The $n=13$ and $n=55$ clusters also underwent strong fragmentation upon ionization. The first nonadiabatic calculation was conducted by Kuntz and Hogreve[12] using the classical-path surface-hopping trajectory method.[13] This study included the lowest three adiabatic states from a diatomics-in-molecules (DIM) model of the electronic Hamiltonian, and interpreted the dissociation of the argon trimer upon ionization in terms of charge migration and nonadiabatic effects. They mainly found dimer fragments, in contrast to the experimental results where monomer ions are also found. The first study taking into account all the potential-energy surfaces involved in the dynamics was carried out for Ar_3 and Ar_4 using a DIM model for the electronic Hamiltonian and mean-field ("hemiquantal") dynamics.[14] The results showed good agreement with experiment, both for the monomer and dimer fragment proportions and for the fact that no Ar_3^+ was observed from Ar_3 ionization and no Ar_3^+ nor Ar_4^+ from Ar_4 ionization.

We have already studied the fragmentation of neon[15] and krypton[16] clusters upon electron-impact ionization, for sizes up to $n=14$ (Ne_n) and 11 (Kr_n), taking into account all the potential-energy surfaces and their couplings, and adding the spin-orbit correction. These simulations have revealed extensive fragmentation of the parent ions, with dimers being the most abundant fragments for all studied sizes. Trimer fragments only began to appear (with a proportion at least about 0.5%) for initial cluster sizes around $n=9$ (Ne_3^+) and 5 (Kr_3^+). In this work we study the fragmentation of argon clusters, $n=2-11$, in order to confront our results with experiment. This is the first attempt to study the effect of electron-impact ionization on neutral argon clusters with sizes exceeding four atoms and treating the multisurface aspect of the dynamics. It is also the first theoretical study attempting a comparison with all the experimental results of Lohbrandt *et al.*[7] We are thus able to test the accuracy of our simulation on the formation of Ar^+, Ar_2^+, and Ar_3^+ fragments. We can also determine the time scale of the fragmentation, giving the first information on the kinetic aspect of this process. In addition, we can address the following question: Since Ar_3^+ constitutes the ionic core in larger clusters, is it going to be the largest fragment?

We use the same method that has already been successfully applied to the dynamics of neon[15] and krypton[16] clusters. The potential-energy surfaces and their couplings are obtained from the DIM model with the addition of the induced dipole-induced dipole and spin-orbit interactions. The mixed quantum-classical molecular dynamics with quantum transitions (MDQT) method of Tully[17] is used for the dynamics, taking into account all the coupled electronic states converging asymptotically to the $Ar^+(^2P_{3/2})$ or $Ar^+(^2P_{1/2})$ $+(n-1)$ Ar dissociation limits. This methodology is presented in Sec. II. Fragment abundances are presented in Sec. III and compared with the experimental ones. Section IV is

TABLE II. Comparison of the dissociation energies D_e (cm^{-1}) and equilibrium internuclear distances R_e (Å) of Ar_2^+ deduced from our fit to the values derived from the *ab initio* calculations of Ha *et al.* (Ref. 23).

		$^2\Sigma^+_{1/2u}$	$^2\Pi_g$	$^2\Pi_u$	$^2\Sigma^+_{1/2g}$
D_e	Ref. 23	11236	1434	283	61
	Our fit	11230	1441	278	66
R_e	Ref. 23	2.4047	3.0242	3.8783	5.7846
	Our fit	2.4033	3.0249	3.8919	5.7701

devoted to the discussion of the comparison between our simulated and the experimental results, and Sec. V to the conclusions.

II. METHOD

A. Potential-energy surfaces

The multidimensional adiabatic potential-energy surfaces of Ar_n^+ clusters are obtained using the same method as in our previous works about the fragmentation of ionized neon[15,18] and krypton[16] clusters. The potential-energy surfaces are described by a DIM model[19–21] based on the HFD-B2 potential of Ar_2 from Ref. 22 and recent *ab initio* calculations[23] for the four lowest Ar_2^+ potentials. The Ar_2^+ *ab initio* points are fitted by analytical curves of the form

$$V(R) = V_{\text{short}}(R) + [V_{\text{long}}(R) - V_{\text{short}}(R)]T(R), \tag{1}$$

where $V_{\text{short}}(R)$ is the short-range interaction taken as

$$V_{\text{short}}(R) = \sum_{n=1}^{2} (A_n e^{-\alpha_n R^n} + B_n e^{-\beta_n/R^n} + D_n e^{-n\delta R}). \tag{2}$$

$V_{\text{long}}(R)$ is the long-range ion-induced dipole interaction

$$V_{\text{long}}(R) = \frac{C_4}{R^4} + \frac{C_6}{R^6} + \frac{C_8}{R^8}, \tag{3}$$

and $T(R)$ is a switching function

$$T(R) = 0.5[1 + \tanh(a(R-b))]. \tag{4}$$

The values of the coefficients resulting from the fit are collected in Table I. Root-mean-square deviations between our fitted curves and *ab initio* points are all below 6 cm^{-1}.[24] The quality of the fit is confirmed by Table II in which the resulting dissociation energies D_e and internuclear distances R_e of Ar_2^+ are compared to the values presented in Ref. 23.

We add the induced dipole-induced dipole interactions[25,26] using an effective polarizability[27] of the form

$$\alpha_{\text{eff}}(R) = R_{\text{pol}}/(\sqrt{R_{\text{pol}}/\alpha} + 1/R)^2 \tag{5}$$

so that this interaction goes to zero at short distances where it is unphysical. In Eq. (5) α is the polarizability of the argon atom[28] ($\alpha = 1.586$ Å$^3 = 10.703$ bohr^3) and R_{pol} is a cutoff distance. A value of $R_{\text{pol}} = 3.545$ bohr has been chosen. This value corresponds to the distance for which $V_{^2\Sigma_u^+(Ar_2^+)}(R_{\text{pol}}) \approx V_{^2\Sigma_u^+(Kr_2^+)}(R'_{\text{pol}})$ where R'_{pol} is the cutoff distance defined for krypton clusters.[27]

The spin-orbit coupling is treated using the semiempirical treatment of Cohen and Schneider,[29] as presented in Ref. 25. The only input parameter is the spin-orbit splitting between the $^2P_{3/2}$ and $^2P_{1/2}$ states of Ar^+, which is equal to 1431.5831 cm^{-1}.[23] A comparison of the dissociation energies D_e and internuclear distances R_e of Ar_2^+ with the inclusion of the spin-orbit interaction is presented in Table III.

B. Dynamical method

The method used in this work has already been applied to the study of ionized neon and krypton clusters.[15,16,18] We briefly recall here its essential features. The ~60 eV electron-impact ionization of neutral argon clusters Ar_n ($2 \leqslant n \leqslant 11$) is modeled by a vertical ionization of the cluster evolving classically in its zero-point vibrational level to a randomly selected electronic state of the ion. The potential-energy minima and harmonic zero-point-level energies (ZPLEs) of neutral argon clusters with sizes up to $n=11$ atoms are reported in Table IV and compared to the minimum energies of Hoare and Pal[30] and to the ZPLE of Leitner *et al.*[31] (harmonic and diffusion quantum Monte Carlo calculations), respectively. As expected from the argon mass, the harmonic approximation is quite suitable for argon clusters. The slight deviations between our results and the ones from the litterature come from the different Ar–Ar interactions used.

The ionized argon cluster dynamics is described using the MDQT method of Tully[17] in which the classical nuclei evolve on one adiabatic surface at a time. Transitions between electronic states are taken into account by allowing for hops between surfaces. Fragments are collected after ensuring that they are stable. An Ar_p^+ fragment ($p \leqslant n$) is assumed

TABLE III. Comparison of the dissociation energies D_e (cm^{-1}) and equilibrium internuclear distances R_e (Å) of Ar_2^+ deduced from our fit to the values derived from the *ab initio* calculations of Ha *et al.* (Ref. 23) when the spin-orbit interaction is included.

				I(1/2)$_g$[a]				
		I(1/2)$_u$	I(3/2)$_g$	(inner well)	(outer well)	I(3/2)$_u$	II(1/2)$_u$	II(1/2)$_g$
D_e	Ref. 23	10778	1434	549	79	283	590	134
	Our fit	10772	1441	556	82	278	586	132
R_e	Ref. 23	2.4047	3.0242	3.0449	5.2745	3.8783	3.6979	4.6865
	Our fit	2.4039	3.0249	3.0424	5.3335	3.8919	3.6944	4.7098

[a]The position of the maximum between the two potential wells is $R_{\max} = 4.120$ Å with $E_{\max} = -20$ cm^{-1} in Ref. 23 and $R_{\max} = 4.1335$ Å with $E_{\max} = -19$ cm^{-1} from our fit.

TABLE IV. Minimum (E_{min}) and zero-point-level energies (ZPLE) of Ar_n in wave numbers and in units of ϵ, the Ar_2 well depth, compared to the minimum energies of Hoare and Pal (Ref. 30) and to the ZPLE of Leitner *et al.* (Ref. 31), respectively (see text). ZPLE are estimated from the harmonic oscillator approximation (HO) in our calculations. The zero for energies is the completely dissociated cluster, i.e., (nAr).

n	E_{min} (cm^{-1}) (This work)	E_{min} (ϵ) (This work)	E_{min} (ϵ) (Ref. 30)	$ZPLE^{HO}$ (cm^{-1}) (This work)	$ZPLE^{HO}$ (ϵ) (This work)	$ZPLE^{HO}$ (ϵ) (Ref. 31)	$ZPLE^{DMC}$ (ϵ) (Ref. 31)
2	−99.546	−1.000	−1.000	−84.0639	−0.8445	−0.8411	−0.8485
3	−298.639	−3.000	−3.000	−252.862	−2.540	−2.530	−2.553
4	−597.277	−6.000	−6.000	−507.044	−5.094	−5.074	−5.113
5	−903.149	−9.073	−9.104	−768.806	−7.723	−7.726	−7.791
6	−1249.83	−12.555	−12.712	−1065.16	−10.700	−10.804	−10.882
7	−1626.98	−16.344	−16.505	−1394.12	−14.005	−14.098	−14.183
8	−1947.18	−19.561	−19.821	−1671.01	−16.786	⋯	⋯
9	−2363.54	−23.743	−24.113	−2034.45	−20.437	⋯	⋯
10	−2778.49	−27.912	−28.422	−2398.65	−24.096	⋯	⋯
11	−3194.60	−32.092	−32.766	−2764.81	−27.774	⋯	⋯

to be stable when its internal energy is below the classical minimum energy of Ar_{p-1}^+. The energy minima and the corresponding configurations of Ar_n^+ clusters up to $n=11$ are presented in Table V and compared to DIM calculations from Ikegami *et al.*,[32] Doltsinis and Knowles,[33] and Hrivňák and Kalus.[34] Our minima are in good agreement with the recent calculations from Ref. 33 and are always below the minima from Ref. 32 and above the minima from Ref. 34. Our most stable configurations are in general found to be the same ones as in Ref. 33 and 34. The only differences correspond to configurations which present a local minimum very close in energy to the global minimum: the energy difference between the $c[4]$ and $c[3]1r[1]$ tetramers and between the $c[3]1r[5]2r[2]$ and $c[3]1r[4]2r[3]$ decamers are equal to 1.6 and 0.4 cm^{-1}, respectively. Unlike results from Ref. 32, the most stable hexamer is found to have only one ring, the configuration with two rings being about 14 cm^{-1} less stable in our calculation. The differences encountered with these earlier works mainly originate from using different Ar_2^+ and Ar_2 potential curves.

TABLE V. Minimum energies of Ar_n^+ without (E_{min}) and with (E_{min}^{SO}) the spin-orbit interaction. Minimum energies and most stable configurations (denoted as c(n)1r[p]2r[q] for a configuration with a n-atom core, a p-atom first ring, and q-atom second ring) without inclusion of the spin-orbit interaction are compared to previous DIM calculations from Ikegami *et al.* (Ref. 32), Doltsinis and Knowles (Ref. 33), and Hrivňák and Kalus (Ref. 34). The zero for energies is the completely dissociated cluster, i.e., $Ar^+(^2P)+(n-1)$ Ar or $Ar^+(^2P_{3/2})+(n-1)$ Ar in the absence or the presence of spin-orbit interaction for ionic clusters.

n	E_{min} configurations (eV) (This work)	E_{min} configurations (eV) (Ref. 32)	E_{min} configurations (eV) (Ref. 33)	E_{min} configurations (eV) (Ref. 34)	E_{min}^{SO} configurations (eV) (this work)
2	−1.392 350	⋯	−1.366	⋯	−1.335 608
	$c[2]$	⋯	$c[2]$	⋯	$c[2]$
3	−1.576 510	−1.558	−1.567	−1.6195	−1.519 717
	$c[3]$	$c[3]$	$c[3]$	$c[3]$	$c[3]$
4	−1.652 694	−1.604	−1.647	−1.6985	−1.595 850
	$c[4]$	$c[3]1r[1]$	$c[3]1r[1]$	$c[3]1r[1]$	$c[4]$
5	−1.739 511	−1.663	−1.738	−1.7854	−1.682 767
	$c[3]1r[2]$	$c[3]1r[2]$	$c[3]1r[2]$	$c[3]1r[2]$	$c[3]1r[2]$
6	−1.827 147	−1.724	−1.831	−1.8720	−1.770 429
	$c[3]1r[3]$	$c[3]1r[2]2r[1]$	$c[3]1r[3]$	$c[3]1r[3]$	$c[3]1r[3]$
7	−1.920 902	−1.795	−1.928	⋯	−1.864 211
	$c[3]1r[2]2r[2]$	$c[3]1r[2]2r[2]$	$c[3]1r[2]2r[2]$	⋯	$c[3]1r[2]2r[2]$
8	−2.013 502	−1.862	−2.025	⋯	−1.956 839
	$c[3]1r[3]2r[2]$	$c[3]1r[3]2r[2]$	$c[3]1r[3]2r[2]$	⋯	$c[3]1r[3]2r[2]$
9	−2.107 565	−1.932	−2.125	⋯	⋯
	$c[3]1r[3]2r[3]$	$c[3]1r[3]2r[3]$	$c[3]1r[3]2r[3]$	⋯	⋯
10	−2.200 000	−2.001	−2.230	⋯	⋯
	$c[3]1r[4]2r[3]$	$c[3]1r[4]2r[3]$	$c[3]1r[5]2r[2]$	⋯	⋯
11	−2.300 629	−2.076	−2.335	⋯	⋯
	$c[3]1r[5]2r[3]$	$c[3]1r[5]2r[3]$	$c[3]1r[5]2r[3]$	⋯	⋯

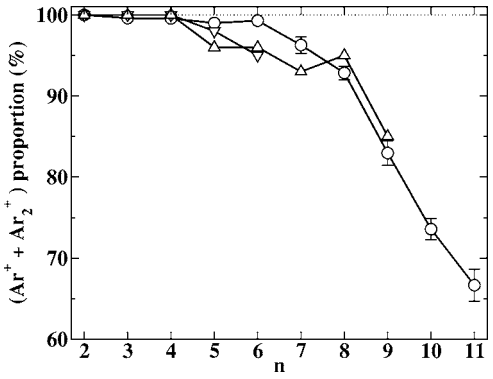

FIG. 1. Sum of the Ar^+ and Ar_2^+ proportions (%) obtained from electron-impact ionization of Ar_n for $n=2$ to 11. Comparison between our simulated results (circles) and the experimental results from Buck and Meyer, Ref. 1, for $n=2-6$ (downward triangles), and from Lohbrandt *et al.*, Ref. 7, for $n=2-9$ (upward triangles).

C. Computational details

The results presented in this paper come from a 100 ps propagation unless otherwise specified. They are averaged over a set of 5000 trajectories for $n \leqslant 9$ and 1000 trajectories for $n=10-11$ when the spin-orbit interaction is not included. When it is included, the averaging is performed over a set of 5000 trajectories for $n=2-4$ and 1000 trajectories for $5 \leqslant n \leqslant 9$. Calculations including the spin-orbit interaction were limited to Ar_n clusters with $2 \leqslant n \leqslant 9$ because of computational cost. Statistical error bars are determined by estimating the root-mean-square deviation between the 10 packets of 500 or 100 trajectories depending on whether the total number of trajectories equals 5000 or 1000. Unless otherwise specified, the results presented in this paper are from our most complex simulations, i.e., including the spin-orbit interaction for $n \leqslant 9$ and not including it for $n=10$ and 11.

Fragmentation occurs when an ionic subcluster has more than 99.9% of the charge and any of its atoms is at least 11 Å away from any of the other neutral atoms. If the subcluster is stable the trajectory is stopped, otherwise it is further propagated for the subcluster only. Finally, the argon ^{40}Ar mass used in this work is $m=39.962\,383\,7$ a.m.u.

III. FRAGMENT ABUNDANCES

A. Overall proportion of the most abundant fragments

Figure 1 shows the sum of the monomer and dimer ionic fragment proportions for $n=2-11$ from our simulation, compared to the experimental results of Buck and Meyer[1] for $n=2-6$ and to the results of Lohbrandt *et al.*[7] for $n=2-9$. Our simulated results are in very good agreement with the experimental ones. They all show extensive fragmentation, since Ar^+ and Ar_2^+ sum up to nearly 100% of the fragments for $n \leqslant 6$, and they still represent more than 65% of the fragments for the largest size studied here, $n=11$. Taking into account the experimental uncertainties,[7] both the experimental and the simulated results show a decrease in the $(Ar^+ + Ar_2^+)$ proportion with initial cluster size.

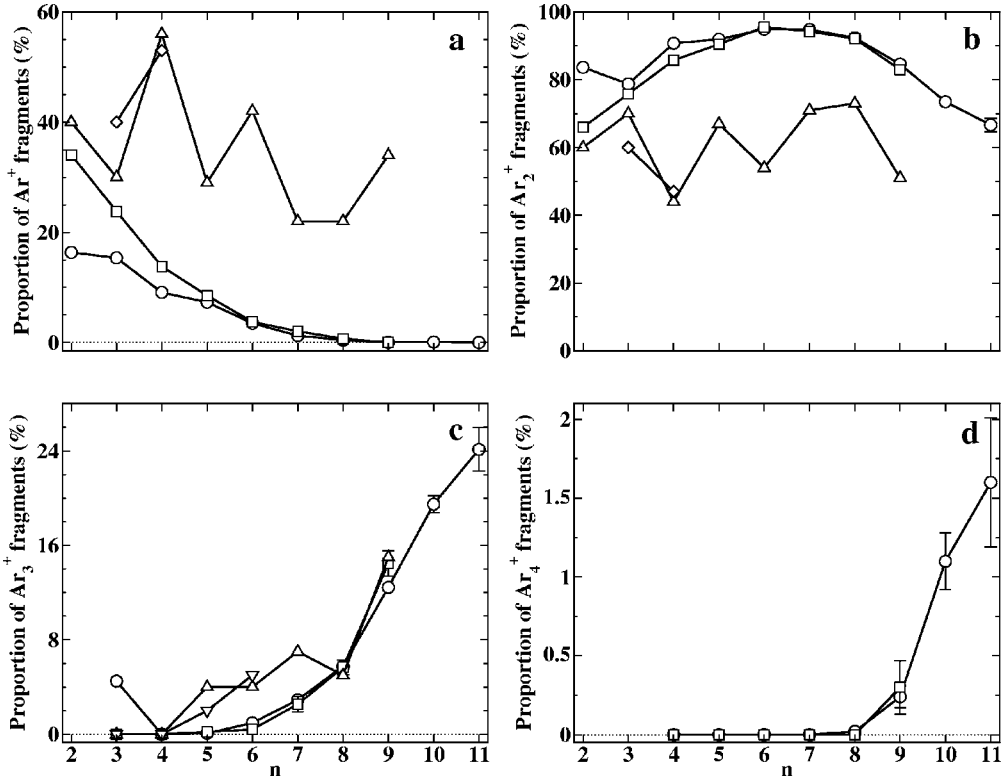

FIG. 2. Proportions (%) of stable (a) Ar^+, (b) Ar_2^+, (c) Ar_3^+, and (d) Ar_4^+ as a function of initial cluster size. Our calculations including (squares) or not (circles) the spin-orbit interaction are compared to available experimental data (downward triangles) from Buck and Meyer, Ref. 1, for $n=2-6$, and from Lohbrandt *et al.*, Ref. 7, for $n=2-9$ (upward triangles). They are also compared to the simulation results of Bastida *et al.* (Ref. 14) (diamonds). The statistical uncertainty is only specified when it exceeds the size of the plotting symbols.

B. Individual fragment proportions

Figure 2 presents a more detailed comparison of the experimental and simulated results. It shows the proportions of the Ar^+, Ar_2^+, Ar_3^+, and Ar_4^+ fragments as a function of the initial cluster size. The agreement is very good concerning the larger fragments, Ar_p^+ with $p=3$ and 4. Our simulation shows that Ar_3^+ starts appearing for $n \geqslant 5$, and then its proportion increases with initial cluster size. This is also true within experimental uncertainties for the results of Lohbrandt *et al.*[7] No Ar_4^+ is produced for initial cluster sizes below $n=9$ in our simulation and Lohbrandt *et al.* did not detect any tetramer ion for $n \leqslant 9$. Ar_2^+ is also found to be the most abundant fragment, which is in agreement with the experiment.

However, there is a striking difference for the proportion of the monomer and dimer ion fragments. Even though the experimental sum of the Ar^+ and Ar_2^+ fragment proportions is in very good agreement with the simulation for $n=2-9$ and decreases smoothly from $n=2$ to 11, as seen in Fig. 1, the individual Ar^+ and Ar_2^+ fragment proportions do not agree. Our simulation shows a systematic, monotonic evolution: The monomer proportion decreases from 34% for $n=2$ to zero for $n=9$, and the dimer one first increases from 66% for $n=2$ to a maximum of 95% for $n=6$, then decreases to 67% for $n=11$. The experimental proportions are in reasonably good agreement for $n=2$ and 3, but then they start to oscillate, with a slight tendency to decrease on average for the monomer and no clear tendency for the dimer. In addition, the experimental proportion of dimer fragments is smaller than our simulated result (and reverse for the monomer) for all studied sizes.

Earlier theoretical results by Bastida *et al.*[14] are also presented in Figs. 2(a) and 2(b) for $n=3$ and 4. Their simulation used potential-energy surfaces and couplings very similar to our model (without the spin-orbit coupling), and a mean-field method for the dynamics. Their results are very close to the experimental ones. Unfortunately they only studied the case of $n=3$ and 4, so it cannot be checked if their results would exhibit the same oscillations as the experimental ones. An extension of this work is currently being performed by Kalus, Gadea, and co-workers.[35] It will be very interesting to see how they compare with the experimental results and with our theoretical results.

Finally, note that the effect of the spin-orbit interaction is important for the smaller cluster sizes. The proportion of Ar^+ fragments is roughly doubled when it is included for Ar_2. Moreover, there is about 4% of Ar_3^+ fragments produced from Ar_3 when the spin-orbit coupling is neglected: this is a unique case where no fragmentation of the parent ion occurs, and it disappears when this coupling is taken into account. This has also been observed in the case of krypton clusters[16] and it is due to the existence of a potential well in one of the A'' states in the Franck Condon region. However, for $n \geqslant 6$ there is almost no difference between the results that do or do not include the spin-orbit correction, which validates our simulation for $n \geqslant 9$ (performed without the inclusion of the spin-orbit coupling).

TABLE VI. Proportions of Ar^+, Ar_2^+, and Ar_3^+ fragments obtained by providing the neutral hexamer its ZPE (first row) and its ZPE plus 162 cm^{-1} (second row). The calculation was performed over a set of 5000 trajectories and the spin-orbit interaction was not taken into account.

	Ar^+	Ar_2^+	Ar_3^+	Time limit reached
ZPE	3.49±0.16	94.91±0.23	0.96±0.12	0.64±0.10
ZPE+162 cm^{-1}	3.21±0.23	95.35±0.34	0.82±0.13	0.62±0.13

C. Effect of the warming of the neutral argon clusters

In the experiment by Buck and Meyer[1] and by Lohbrandt *et al.*[7] the initial step in the size selection of the neutral clusters consists in crossing a 567 m/s argon beam with a 1790 m/s helium beam. This collisional process is not sufficient to dissociate the neutral clusters experimentally, except for the dimers. But it can result in a warming of the neutral clusters which can in turn have an influence on the fragmentation process. We have studied this effect for Ar_6. Using the same model as Buck and Meyer,[1,36] we have estimated a maximum amount of energy transfer of 162 cm^{-1}. Table VI presents the fragment proportions obtained by providing the neutral hexamer its zero-point energy (ZPE) and its ZPE plus 162 cm^{-1}. The results are quite similar in both cases, which shows that the increase in the initial neutral cluster energy does not influence the final fragment proportions. This confirms the assumption made by Buck and Meyer,[1] as well as the results we have previously obtained on neon[15] and krypton[16] clusters.

D. "Forbidden" transitions and lifetime of the Ar_2^+ $II(1/2)_u$ state

In our calculations that do include the spin-orbit coupling, the $II(1/2)_u$ state of Ar_2^+ decays to the $I(1/2)_u$ state in about 3.5 ps whenever it is populated in our simulation (mostly for small initial sizes). This seems to be in contradiction with the commonly accepted microsecond range value for rare-gas dimer ions. The Ar_2^+ $II(1/2)_u$ value was determined to be 47 μs by Norwood *et al.*[37] in a photoion-photoelectron coincidence (PIPECO) study of Ar_n, $n=2-4$. Lepère *et al.*[38] have measured lifetimes between 60 and 70 μs depending on the size of the neutral parents. However, the discrepancy could be explained when considering the role of autoionizing processes. The Ar_2^+ $II(1/2)_u$ observed experimentally could originate from autoionizing states which keep producing them on a microsecond time scale. In a spectroscopy experiment conducted by Rupper and Merkt,[39] the Ar_2^+ $II(1/2)_u$ linewidths are of the order of 1 cm^{-1}. This is probably the limit of their experimental resolution, but it is compatible with a 5 ps lifetime. In addition, Carrington and Softley[40] have observed lifetimes in the 150 ps to 2.8 ns range for $HeNe^+$ for both the $v=0$ and $v=1$ levels of the $A_2\ ^2\Pi_{1/2}$ state correlating to the $Ne^+(^2P_{1/2})+He(^1S)$ dissociation limit. Hence electronic predissociation due to spin-orbit coupling can be very efficient even in the absence of a potential crossing or avoided crossing.

This is also true for the spin-orbit induced decay of the $II(1/2)_g$ to the $I(1/2)_g$ state. For the 34% trajectories that do not dissociate directly (this state is mainly repulsive except

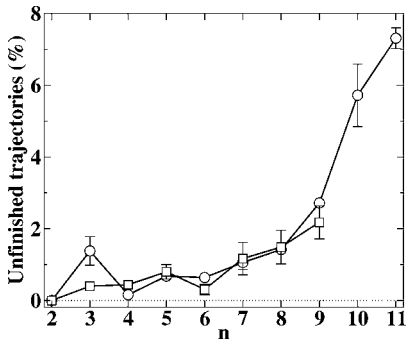

FIG. 3. Proportion of trajectories that have reached the 100 ps time limit as a function of the initial cluster size, for simulations where the spin-orbit interaction is taken (squares) or not taken (circles) into account. The statistical uncertainty is only specified when it exceeds the size of plotting symbols.

for a small Van der Waals well), the decay lifetime is about 0.1 ps which can be compared with the 19 ps lifetime determined for the same state of Kr_2^+.[16]

IV. DISCUSSION

A. Long-lived trajectories

The fragment proportions presented in Fig. 2 do not sum up to 100%, especially for the larger clusters. This is due to the existence of trajectories that have not led to stable fragments at the 100 ps time limit. The proportion of these unfinished trajectories increases with respect to the initial cluster size, as can be seen from Fig. 3. It is negligible for $n=2$, and reaches 7.5% for $n=11$. This is too small to explain the discrepancy between simulation and experiment. However, these long-lived trajectories could explain slight quantitative discrepancies observed for Ar_3^+ proportions in Fig. 2(c). As shown in a recent work on krypton clusters,[16] they correspond to intermediate species trapped in low-energy states (mainly the ground electronic state), and they tend to favor the production of larger fragments. The same behavior is found here. The increase in the proportion of long-lived trajectories for $n \geqslant 7$ (Fig. 3) coincides with the production of Ar_3^+ and Ar_4^+ fragments [Figs. 2(c) and 2(d)]. We have checked for Ar_9 that long-lived trajectories do lead to the production of larger fragments, by further propagating them adiabatically for 1 and 10 ns. The results are reported in Table VII. The Ar_3^+ and Ar_4^+ fragments are clearly more abundant, and no Ar^+ is produced. However, taking into account the contribution of these trajectories will only increase the proportion of the larger fragments (Ar_3^+ and Ar_4^+) for initial cluster sizes $n \geqslant 9$, given that they are rather scarce for smaller clusters.

B. Comparison of the monomer and dimer proportions with experiment

1. Electronic states reached by electron-impact ionization

The main difference between our simulation and the experimental results is the large and oscillating proportion of monomer fragments observed experimentally, whereas our results show a monotonically decreasing proportion with cluster size. Larger proportions of monomer fragments could be obtained in our simulation if electron-impact ionization did not produce a uniform distribution of the parent ion electronic states. We have assumed, as is usual, that electrons with an incident energy of 50 eV or more equiprobably populate all the electronic states of the parent ion $(Ar_n^+)^*$ going asymptotically to $Ar^+(^2P)+(n-1)$ Ar. If some of the electronic states were preferentially populated, the fragment abundances would be affected. For instance, we have shown in our recent work on neon[41] and on krypton clusters[16] that monomer fragments originate from trajectories initiated on the highest electronic states. However, even assuming that only the highest electronic states were populated would not be sufficient to give a large proportion of monomer fragments. For instance, Fig. 4 shows the fragment abundances obtained from $(Ar_9^+)^*$ as a function of the state number on which dynamics has started. Even the upmost state leads to less than 1% of Ar^+, which is much smaller than the 34% experimental proportion.

Another possibility to get a larger proportion of Ar^+ fragments would be the production of higher excited states in the ionization process. All the states that correlate with $Ar^+(^2P_{3/2})+(n-1)$ Ar and $Ar^+(^2P_{1/2})+(n-1)$ Ar are included in our simulation. The next higher states in energy are the electronic states that correlate with $Ar^+(^2S)+(n-1)$ Ar (which correspond to a hole in a $3s$ orbital). They would certainly lead to more extensive fragmentation since they lie about 13 eV higher in energy. However, the electron-impact

TABLE VII. Fragment abundances (%) after 1 and 10 ns further propagation of long-lived trajectories for Ar_9, compared to fragment abundances at the end of the 100 ps simulation. The first three rows present fragment abundances normalized over the whole set of trajectories (5000 trajectories) whereas the three last rows correspond to a normalization over the long-lived trajectories only (136 trajectories).

Propagation time interval	Ar^+	Ar_2^+	Ar_3^+	Ar_4^+	Time limit reached
Analysis of the 5000 trajectories					
[0, 100 ps]	0.04	84.56	12.44	0.24	2.72
[0, 1.1 ns]	0.04	85.74	12.90	0.36	0.96
[0, 10.1 ns]	0.04	85.93	13.09	0.38	0.56
Analysis of the 136 unfinished trajectories (2.72%)					
@ 100 ps	0	0	0	0	100
[100 ps, 1.1 ns]	0	43.38	16.91	4.41	35.29
[100 ps, 10.1 ns]	0	50.76	24.24	5.30	19.70

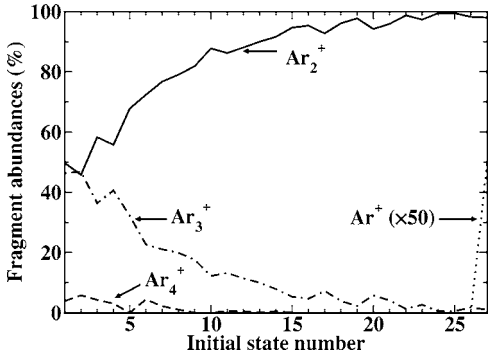

FIG. 4. Fragment abundances with respect to the initial state number on which the dynamics begins for Ar_9 without inclusion of the spin-orbit coupling. These abundances are normalized to 100% for each state. Note that the Ar^+ proportion is multiplied by 50.

ionization cross section of Ar to $Ar^+(^2S)$ is about 15 to 30 times lower than that to $Ar^+(^2P)$ for incident electron energies between 50 and 150 eV.[42] Assuming the same ratio for the ionization cross sections in the cluster, the ionization to electronic states correlating to $Ar^+(^2S)+(n-1)$ Ar could only add about 5% of Ar^+ fragments at most, which is far less than the difference between our results and the experimental ones for $4 \leqslant n \leqslant 9$.

2. Parent ion lifetimes and possibility for secondary ionization

One possibility for explaining why the experimental results show more monomer fragments could be the ionization of neutral monomers produced in the electron bombardment region, that is, once the neutral cluster size selection has been performed. This could occur if the dissociation of the parent ions is very fast, i.e., faster than the time it takes for clusters to travel out of the electron bombardment region (of the order of 1.8 μs assuming that the velocity of the argon cluster beam is unchanged after the collision with the helium beam and that the electron bombardment region is about 1 mm long). Figure 5 presents the parent ion lifetimes (defined as the lifetime for the first fragmentation) for cluster sizes up to 11 atoms. These lifetimes are all of the order of 1 ps or less. In addition, Table VIII reports the time constants t_{form} characterizing the appearance of the most abundant fragments, Ar_2^+, and the times $t_{stab}(X\%)$ needed to stabilize at

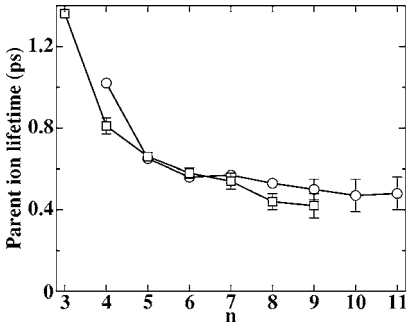

FIG. 5. Decay lifetimes in picoseconds of the $(Ar_n^+)^*$ parent ions as a function of their size, with (squares) and without (circles) inclusion of the spin-orbit coupling. Uncertainties are only specified when their magnitude exceeds the size of plotting symbols.

TABLE VIII. Stabilization times t_{stab} and time constants t_{form} in picoseconds for the most abundant fragment, namely, Ar_2^+, coming from the fragmentation of $(Ar_4^+)^*$, $(Ar_6^+)^*$, and $(Ar_8^+)^*$ parent ions, evaluated with or without the inclusion of the spin-orbit interaction (SO).

Initial neutral cluster	t_{form}	t_{stab} (1%)	t_{stab} (2%)
Ar_4	2.02±0.07	14	10
Ar_6	2.76±0.05	25	18
Ar_8	4.23±0.05	39	30
Ar_4(+SO)	1.71±0.05	11	9
Ar_6(+SO)	2.70±0.05	30	17
Ar_8(+SO)	4.16±0.06	47	32

least $(100-X)\%$ of Ar_2^+ fragments (see Ref. 16 for a more detailed definition). As can be seen from this table, 99% of the final fragments are obtained within 50 ps at most. This is very fast compared to the time taken by clusters to travel out of the electron bombardment region. Fragmentation mostly proceeds by the ejection of neutral atoms (possibly several ones at the same time). It is therefore reasonable to assume that some of these neutral argon atoms can be ionized before they leave the ionization region. However, the importance of this process is difficult to estimate since it depends on the electron flux and on the ionization cross section of argon monomers (about 2.5 $Å^2$ in the 50–100 eV range[43]).

V. CONCLUSIONS

We have performed a mixed quantum-classical study on the fragmentation dynamics of neutral argon clusters Ar_n $(2 \leqslant n \leqslant 11)$ following electron-impact ionization. Our results show fast (picosecond time scale) and extensive fragmentation. The most abundant ionic fragments are Ar^+ and Ar_2^+, which sum up close to 100% of the fragments for $n < 6$. Ar_3^+ fragments only start appearing for initial cluster sizes $n=5$ or more. These results are in very good agreement with the experimental findings of Buck and Meyer[1] and of Lohbrandt *et al.*[7] However, the individual Ar^+ and Ar_2^+ proportions reveal a striking difference. Our simulation shows a systematic, monotonic evolution, with the monomer proportion decreasing smoothly from $n=2$ to 9 and the dimer proportion increasing from $n=2$ to a maximum for $n=6$ then decreasing again. They are in good agreement with the experimental proportions for $n=2$ and 3, but then the experimental monomer and dimer fragment proportions start oscillating. The monomer fragment proportion does show a tendency to decrease on average with cluster size, but the experimental result is larger than ours for all studied sizes. This difference could be attributed to the approximate character of our simulation. However, the method used here has given very good results in a number of studies. It would be very useful in that respect to compare with the results of a simulation currently being performed with mean-field techniques by Kalus *et al.*. Another possibility could be a process that is not taken into account in our simulation, such as the secondary ionization of neutral fragments coming from the dissociating ionized cluster. Further studies will be needed to elucidate this difference. Finally, we have found a fast spin-orbit-induced decay of the $\Pi(1/2)_u$ and $\Pi(1/2)_g$ states of

Ar_2^+. The discrepancy with experimental lifetimes could be resolved by taking into account the role of autoionizing states in the formation of the parent ions.

ACKNOWLEDGMENTS

The authors would like to thank U. Buck and M. Fárník for fruitful discussions and strong interest in this work. The Calmip computer center of Toulouse and the IDRIS national computer center of Paris are gratefully acknowledged for a grant of computer time. The Chemistry Department of CNRS is gratefully acknowledged for additional support to the European COST Project No. D26/0006/02 "Dynamics of nonadiabatic processes."

[1] U. Buck and H. Meyer, J. Chem. Phys. **84**, 4854 (1986).
[2] H. Haberland, Surf. Sci. **156**, 305 (1985).
[3] U. Buck and H. Meyer, Phys. Rev. Lett. **52**, 109 (1984).
[4] H. Haberland, in *Electronic and Atomic Collisions*, edited by J. Eichler, L. V. Hertel, and N. Stolterfoht (North Holland, Amsterdam, 1983).
[5] T. D. Märk, in *Linking the Gaseous and Condensed Phases of Matter*, edited by L. G. Christophorou, W. F. Schmidt, and E. Illenberger, NATO Advanced Studies Institute Series (Plenum, New York, 1994), p. 155, and references cited therein.
[6] O. F. Hagena, Rev. Sci. Instrum. **63**, 2374 (1992).
[7] P. Lohbrandt, R. Galonska, H. Kim, M. Schmidt, C. Lauenstein, and U. Buck, in *Atomic and Molecular Beams: The State of the Art 2000*, edited by R. Campargue (Springer, Berlin, 2000), pp. 623–636.
[8] C. Steinbach, M. Fárník, U. Buck, C. A. Brindle, and K. C. Janda (private communication).
[9] J. M. Soler, J. J. Sáenz, N. Garcia, and O. Echt, Chem. Phys. Lett. **109**, 71 (1984).
[10] J. J. Sáenz, J. M. Soler, and N. García, Surf. Sci. **156**, 121 (1985).
[11] P. Stampfli, Z. Phys. D: At., Mol. Clusters **40**, 345 (1997).
[12] P. J. Kuntz and J. J. Hogreve, J. Chem. Phys. **95**, 156 (1991).
[13] P. J. Kuntz, J. Chem. Phys. **95**, 141 (1991).
[14] A. Bastida, N. Halberstadt, J. A. Beswick, F. X. Gadéa, U. Buck, R. Galonska, and C. Lauenstein, Chem. Phys. Lett. **249**, 1 (1996).
[15] D. Bonhommeau, A. Viel, and N. Halberstadt, J. Chem. Phys. **123**, 054316 (2005).
[16] D. Bonhommeau, T. Bouissou, N. Halberstadt, and A. Viel, J. Chem. Phys. **124**, 164308 (2006).
[17] J. C. Tully, J. Chem. Phys. **93**, 1061 (1990).
[18] D. Bonhommeau, A. Viel, and N. Halberstadt, J. Chem. Phys. **120**, 11359 (2004).
[19] P. J. Kuntz and J. Valldorf, Z. Phys. D: At., Mol. Clusters **8**, 195 (1988).
[20] F. O. Ellison, J. Am. Chem. Soc. **85**, 3540 (1963).
[21] F. O. Ellison, N. T. Huff, and J. C. Patel, J. Am. Chem. Soc. **85**, 3544 (1963).
[22] R. A. Aziz and M. J. Slaman, Mol. Phys. **58**, 679 (1986).
[23] T. H. Ha, P. Rupper, A. Wüest, and F. Merkt, Mol. Phys. **101**, 827 (2003).
[24] Root-mean-square deviations corresponding to the $^2\Pi_u$ and $^2\Sigma_g^+$ states are estimated by removing the *ab initio* points $R=3.6$, 4.0, and 4.2 a.u. for the $^2\Pi_u$ state and $R=3.6$ a.u. for the $^2\Sigma_g^+$ state.
[25] M. Amarouche, G. Durand, and J. P. Malrieu, J. Chem. Phys. **88**, 1010 (1988).
[26] F. Y. Naumkin and D. J. Wales, Mol. Phys. **93**, 633 (1998).
[27] R. Kalus, I. Paidarová, P. Paska, and F. X. Gadéa, Chem. Phys. **298**, 155 (2004).
[28] *CRC Handbook of Chemistry and Physics*, 81th ed., edited by D. R. Lide (CRC, Boca Raton, 2000).
[29] J. S. Cohen and B. Schneider, J. Chem. Phys. **61**, 3230 (1974).
[30] M. R. Hoare and P. Pal, Adv. Phys. **20**, 161 (1971).
[31] D. M. Leitner, J. D. Doll, and R. M. Whitnell, J. Chem. Phys. **94**, 6644 (1991).
[32] T. Ikegami, T. Kondow, and S. Iwata, J. Chem. Phys. **98**, 3038 (1993).
[33] N. L. Doltsinis and P. J. Knowles, Mol. Phys. **94**, 981 (1998).
[34] D. Hrivňák and R. Kalus, Chem. Phys. **264**, 319 (2001).
[35] R. Kalus (private communication).
[36] U. Buck, J. Phys. Chem. **92**, 1023 (1988).
[37] K. Norwood, J. H. Guo, and C. Y. Ng, J. Chem. Phys. **90**, 2995 (1989).
[38] V. Lepère, I. M. Ismail, M. Barat, J. A. Fayeton, Y. J. Picard, K. Wohrer, C. Jouvet, and S. Martrenchard, J. Chem. Phys. **123**, 174307 (2005).
[39] P. Rupper and F. Merkt, J. Chem. Phys. **117**, 4264 (2002).
[40] A. Carrington and T. P. Softley, Chem. Phys. **92**, 199 (1985).
[41] D. Bonhommeau, N. Halberstadt, and A. Viel, J. Chem. Phys. **124**, 024328 (2006).
[42] P. L. Bartlett and A. T. Stelbovics, Phys. Rev. A **66**, 012707 (2002).
[43] P. McCallion, M. B. Shah, and H. B. Gilbody, J. Phys. B **25**, 1061 (1992).